

Dichroic Measurements on Dicationic and Tetracationic Porphyrins on Clay Surfaces with Visible-Light-Attenuated Total Reflectance

Miharu Eguchi,[1,2] Hiroshi Tachibana,[1] Shinsuke Takagi,*[1] Donald A. Tryk,[1] and Haruo Inoue*[1,3]

[1]Department of Applied Chemistry, Graduate Course of Urban Environmental Sciences, Tokyo Metropolitan University, 1-1 Minami-Ohsawa, Hachiohji, Tokyo 192-0397

[2]JSPS (Japan Society for the Promotion of Science)

[3]SORST, JST (Japan Science and Technology)

Received October 17, 2006; E-mail: inoue-haruo@c.metro-u.ac.jp

Complexes formed with synthetic clay minerals and dicationic and tetracationic porphyrins were prepared. The Soret bands of the multicationic porphyrins shifted to longer wavelength upon the formation of a complex with clay. The clay sheets themselves and the porphyrin molecules on the clay surface were examined by use of atomic force microscopy (AFM) and polarized visible-light-attenuated total reflectance (ATR) spectroscopy (PV-ATR) with a waveguide system. The flat adsorption of the clay sheets on the glass substrates was confirmed by AFM. A theoretical treatment of the analysis by ATR spectroscopy was derived. The orientations of the multicationic porphyrin molecules on the clay sheets in water turned out to be nearly parallel ($<5^\circ$) to the clay surface, based on the PV-ATR analysis.

Inorganic layered materials, such as clay minerals, are fascinating materials. For instance, they provide an extremely flat reaction platform with a wide area.[1–7] AFM observations of clay sheets on flat substrates, such as mica, have been carried out by several researchers.[8–12] Since clay surfaces can be either negatively or positively charged, complex formation via electrostatic interactions with charged organic molecules is facile.

Recently, clay–dye complexes have been extensively studied as functional materials. The photochemical properties of dyes on clay sheets have been reported.[1–7] Dyes, such as porphyrin derivatives,[13,14] sometimes exhibit large bathochromic shifts on the clay sheet, due to changes in conformation that can occur upon adsorption.[15–17] In the case of methylviologen, the fluorescence quantum yield on the clay surface is much larger than that in solution, presumably also due to changes in its conformation.[18,19]

In order to make further progress in the development of photo-induced functions of these types of systems, it is necessary to be able to more fully characterize the surface coverages and molecular orientations. For example, we have recently reported that tetrakis(1-methylpyridinium-4-yl)porphyrin (H_2-TMPyP) does not aggregate on the clay complex up to 100% adsorption vs. the cation-exchange capacity (CEC) of the clay.[17,20–22] Above 100% adsorption, no further H_2TMPyP can adsorb on the clay surface, and the excess exists simply as unaggregated molecules in the bulk aqueous solution. The excited singlet lifetime of the porphyrin on the clay surface is estimated to be on the order of nanoseconds, which is similar to that of the unaggregated porphyrin in solution.[17] Based on the results of these studies, which included both static and dynamic absorption and fluorescence measurements, it has been concluded that the H_2TMPyP molecule forms a monolayer on the clay surface, with negligible aggregation. However, the information that was obtained was insufficient to precisely establish the orientation of the porphyrin on the clay surface.

In general, little is known about the orientations of dyes on clay surfaces, although more is known in the case of dyes intercalated within stacked clay sheets than in the case of exfoliated clay sheets. For example, the orientation angles of incorporated molecules with respect to stacked clay sheets have been estimated using X-ray diffraction (XRD) measurements.[23]

In the present study, the orientations of dicationic and tetracationic porphyrins on exfoliated clay sheets, the latter being adsorbed as monolayers on mica and flat quartz glass, were investigated by the use of atomic force microscopy (AFM)[24,25] and polarized visible-light-attenuated total reflectance (PV-ATR) spectroscopy. Polarized light spectroscopy[26–50] is one of the best techniques with which to determine the molecular orientation. For the PV-ATR measurement, highly flat quartz glass plates (thickness, 0.2 mm) were used. The monitored light beam incident on one lateral surface is totally reflected within the top and bottom surfaces of the quartz glass plate, and finally exits from the opposite lateral surface. Evanescent wave is generated close to the surfaces of the glass plate during each light reflection, and ATR spectroscopy utilizes this light, which is partly absorbed by molecules that are located in this surface region.[29–32,37] Since dozens of total reflections enhance the absorption sensitivity in the waveguide system, and it becomes possible to detect the absorption spectra of porphyrin monolayers adsorbed on the clay surface. The porphyrin ring orientation angle with respect to the glass surface (and thus to the clay surface plane) was quantitatively analyzed in this way.

Experimental

Clay Minerals. Smecton SA (SSA, a synthetic saponite, $Na_{0.77}Mg_{5.97}Al_{0.83}Si_{7.2}O_{20}(OH)_4$) was received from Kunimine Industries Co., Ltd. It was purified by repeated decantation from

Published on the web July 11, 2007; doi:10.1246/bcsj.80.1350

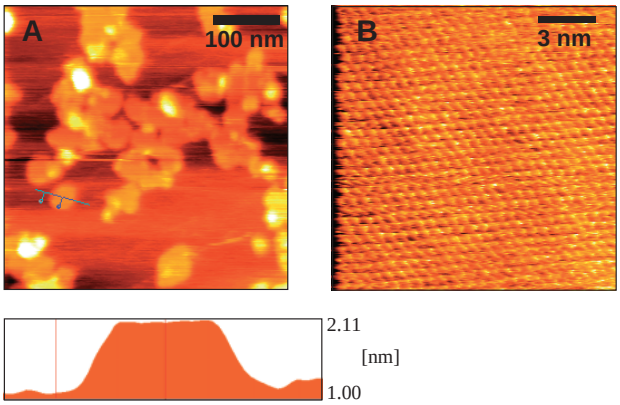

Fig. 1. AFM image (contact mode) of SSA on mica (A), and its enlarged surface (B).

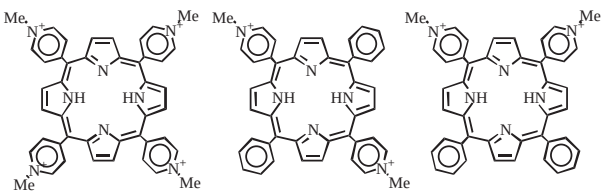

Fig. 2. Structures of multicationic porphyrins.

water and washed with ethanol. The cation exchange capacity (CEC) was 99.7 meq/100 g. From the latter value, together with the theoretical surface area (750 $m^2 g^{-1}$), the average area per anionic site was calculated to be 1.25 nm^2. Thus, the mean distance between the adjacent anionic sites was estimated to be 1.20 nm, on the basis of a hexagonal array.[17,21] The particle size was in the range of 20–50 nm, according to the AFM observations (Fig. 1A). The thickness of the clay sheet is theoretically 0.96 nm. The existence of several water layers between the mica substrate and the clay sheet would enlarge the observed thickness (1.0–1.5 nm). Since the hexagonal array of lattice can be seen over a wide area, the surface of each sheet is extremely flat, even at the atomic level (Fig. 1B). The distance between the bright spots in the AFM image was 0.52 nm. This distance corresponds to the *a*-axis repeat unit of the clay lattice. The amount of water in the SSA was measured by using a thermogravimetric differential thermal analysis (TG/DTA) system (Shimadzu DTG-60H). The weight of the clay mineral was corrected according to the TG measurements.

Porphyrin Derivatives. Tetrakis(1-methylpyridinium-4-yl)-porphyrin (TMPyP) was used as the tetracationic porphyrin. It was purchased from Aldrich, and the counter ion was replaced with chloride on an ion-exchange column (ORGANO AMBERLITE IRA400JCL). Two additional porphyrins, *cis*-bis(*N*-methylpyridinium-4-yl)diphenylporphyrin (*cis*-DPyP) and *trans*-bis(*N*-methylpyridinium-4-yl)diphenylporphyrin (*trans*-DPyP) were used as dicationic porphyrins; these were purchased from Mid-Century Chemicals (Fig. 2). The purity was checked with TLC. The amount of water in the porphyrin was measured by using TG/DTA. The molecular weight was corrected according to the TG measurements.

Solvents. Water was deionized just before use with an ORGANO BB-5A system (PF filter X2 + G-10 column).

AFM Measurements. SPI4000 and SPA300HV systems (Seiko Instruments, Inc.) were used. Cantilevers were purchased from Seiko Instruments, Inc. Super-sharp tips were used for dynamic force mode measurements. The cantilever (Si_3N_4) spring constant was 0.08 N m^{-1} for the contact mode and 20 N m^{-1} for the dynamic force mode. Mica substrates were purchased from Nisshin EM. Glass micro-cover slips were purchased from Matsunami (24 × 24 mm; thickness, 0.12–0.17 mm).

PV-ATR Measurements. A surface-interface spectrometer (System Instruments SIS-50BS) was used. A glass plate waveguide was purchased from System Instruments. The thickness of the glass plate was 0.2 mm; both edges on opposite sides were cut at 60° angles. Under typical conditions, the number of reflections in the waveguide was estimated to be 55. The surface of the waveguide was treated with conc. sulfuric acid to enhance the hydrophilicity of the glass. The glass surface was rinsed with 1 M NaOH, then 1 M HCl, and finally, copious amounts of ion-exchanged water in order to remove excess protons from the glass surface. Cast films for dichroic measurements were prepared as follows. An aqueous solution (3.5 μL) containing nano-layered compound (nano-layered compound: 1.0×10^{-4} equiv L^{-1}) was pipetted onto the hydrophilic quartz waveguide and allowed to air-dry at room temperature. Subsequently, porphyrin aqueous solution (1.0×10^{-5} M, 3.5 μL) was pipetted onto the cast nano-layered compound film, and the excess was washed away with deionized water. The area on the quartz waveguide covered with the complex was around 1.5 cm^2. Thus, samples with the porphyrin–clay complex mostly adsorbed on the waveguide as a monolayer and oriented parallel to the waveguide were prepared.

Absorption Spectra. Absorption spectra were obtained on Shimadzu UV-2550 and UV-3100 UV–visible spectrophotometers.

Results and Discussion

Absorption Spectra of Dicationic and Tetracationic Porphyrins on the Clay Surface. The absorption spectra of porphyrin–clay complexes were measured in water. The concentrations of SSA and porphyrin were 5.0×10^{-4} equiv L^{-1} and 1.0×10^{-5} M, respectively. While the λ_{max} of TMPyP was 421 nm without clay, the value was 451 nm on the clay surface. This spectral shift has been reported previously.[15–17,20–22] The spectral change associated with TMPyP was explained in terms of a flattening of the porphyrin molecule on the clay sheet, that is, the four cationic methylpyridinium moieties become parallel to the porphyrin ring.[15] TMPyP has been thought to adsorb on the clay surface with a parallel orientation with respect to the clay surface, with a four-point electrostatic interaction. Since the clay surface is very flat, the TMPyP molecule becomes flat so as to strengthen the electrostatic interaction. The Na^+ ion, which is originally adsorbed on the clay surface, is replaced by the porphyrin, and should dissolve freely in the bulk aqueous solution. The absorption spectra of *cis*-DPyP are shown in Fig. 3. While the λ_{max} of *cis*-DPyP was 419 nm without clay, it was 455 nm on the clay surface. *trans*-DPyP exhibits a spectral shift from 418 to 447 nm as a result of the complex formation with clay. The spectral changes were +30, +36, and +29 nm for TMPyP, *cis*-DPyP, and *trans*-DPyP, respectively. Since these three porphyrins showed similar spectral changes as a result of complex formation, the adsorption orientations should be similar, that is, all of these porphyrins should adsorb on the clay surface with a parallel orientation with respect to the clay surface in water. However, it has been difficult to determine the adsorption orientations of porphyins on clay surfaces in detail.

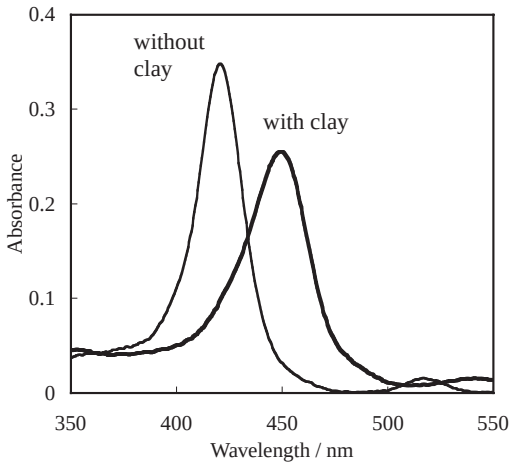

Fig. 3. Absorption spectra of *cis*-DPyP with and without the clay in water. The concentrations of SSA and porphyrin were 5.0×10^{-4} equiv L^{-1} and 1.0×10^{-5} M, respectively.

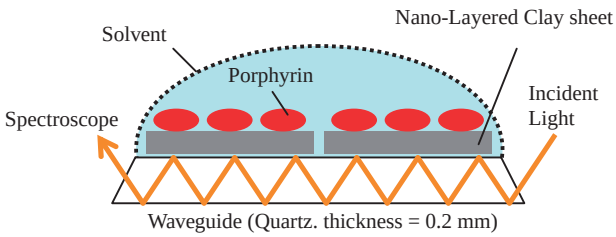

Fig. 4. Setup for visible-light-ATR spectroscopy on a quartz waveguide system. In the actual experimental condition, dozens of total reflections enhance the absorption sensitivity in the waveguide system.

Dichroic measurements should be promising for establishing the porphyrin orientation on the clay surface.

Visible-Light-ATR (Vis-ATR) Spectroscopy of the Clay–Porphyrin Complex on the Quartz Waveguide. In order to determine the adsorption orientation of porphyrin on clay, we examined the visible-light-ATR (Vis-ATR) spectroscopy of the clay–porphyrin complex on the quartz waveguide. Since the clay sheet was adsorbed on the quartz with a parallel orientation, it is possible to measure the porphyrin orientation with respect to the clay surface precisely. Since the clay sheets in a multi-layer film would not be able to retain a perfectly parallel orientation with respect to the glass substrate, a monolayer of clay sheets is much more desirable in order to obtain precise information on the porphyrin orientation. Since dozens of total reflections enhance the absorption sensitivity in the waveguide system, it is possible to measure the absorption spectra of clay–porphyrin monolayer samples. The Vis-ATR-quartz waveguide spectroscopic system, shown in Fig. 4, was used to measure the absorption spectra of single sheets of clay–porphyrin complex. The absence of stacking of clay sheets on the waveguide glass was confirmed by AFM observations before measuring Vis-ATR. The AFM images in different areas of the sample were carefully observed to confirm the absence of stacking of the clay sheets. A Vis-ATR spectrum of the TMPyP–clay complex covered with water is shown in Fig. 5. The spectrum obtained ($\lambda_{max} = 451$ nm) coincides well with

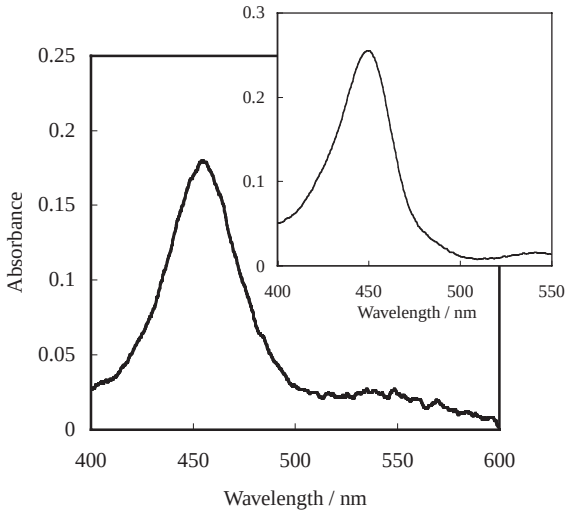

Fig. 5. A Vis-ATR spectrum of a porphyrin (TMPyP) adsorbed on the clay monolayer covered with water on waveguide quartz glass. Inset: absorption spectrum of the clay–porphyrin complex, in which the clay sheets were exfoliated in water.

that obtained for exfoliated clay dispersed in water. If the clay sheets are stacked on the waveguide and TMPyP is intercalated within the clay layer space, the λ_{max} of the porphyrin should be 484 nm.[15–17] If the TMPyP is intercalated between the clay sheets and waveguide glass, the λ_{max} of the porphyrin should be also near 484 nm. However, there was no peak at around 484 nm in the Vis-ATR spectrum (Fig. 5). When a porphyrin solution without clay containing the same concentration with that of clay–porphyrin complex in the above experiment was put on the waveguide, almost no light absorption was observed. This was to verify that only the sample directly adsorbed on the clay attaching to waveguide glass could be observed, since the evanescent light in the visible region exists only within a few hundred nanometers from the waveguide surface. These results indicate that the absorption spectrum observed in Fig. 5 was indeed that of the porphyrin directly adsorbed on the clay monolayer, which was in turn adsorbed in a perfectly flat orientation on the waveguide.

Determination of Porphyrin Orientation on the Clay Surface by Polarized Visible-Light-ATR (PV-ATR) Spectroscopy. PV-ATR spectroscopy was used to determine quantitatively the orientation angle of the porphyrin with respect to the clay surface. The setup and system of coordinates for the polarized spectroscopy are shown in Fig. 6. The incident angle (ϕ) was set at 75°. The reflectance of s- and p-polarized light were calculated by using Fresnel's theory. From the theory, the difference in their reflectance is less than 1% under these conditions. In this experiment, the s- and p-polarized light intensity without sample were observed to determine the correction coefficient due to the difference in the monitoring light intensity of the two types of polarized light. Under the present conditions, the intensity of p-polarized light was 9.6% greater than that of s-polarized light. Thus, the polarized light absorption spectra were corrected accordingly.

The corrected PV-ATR spectra of the TMPyP–clay complex are shown in Fig. 7. The absorbance due to s-polarized light

was significantly larger than that due to p-polarized light. The dichroic ratio (A_p/A_s) at the Soret band was calculated to be 0.16. From these results, the angle of the porphyrin transition moment can be estimated quantitatively.

In a similar way, the PV-ATR spectrum of the clay–*cis*-DPyP complex on a waveguide covered with water was observed (Fig. 8). The absorbance with s-polarized light was much larger than that with p-polarized light. Interestingly, the *cis*-DPyP–clay complex even exhibited a similar A_p/A_s (0.13), compared to the TMPyP–clay complex. Even though *cis*-DPyP has only two cationic sites in the molecule, it turns out that its adsorption orientation on the clay surface is very similar to that of TMPyP, which has four cationic sites. Similar results were also obtained for the *trans*-DPyP–clay complex, also with two cationic sites.

These results qualitatively indicate that the tetracationic and dicationic porphyrins adsorb on the nano-layer clay surface with an orientation almost parallel to the clay surface in water. The actual orientation angle of the porphyrin molecule can be estimated from A_p/A_s at λ_{max}. In order to determine the orientation angle of the porphyrin molecules to the clay surface, we derived an equation (see later).

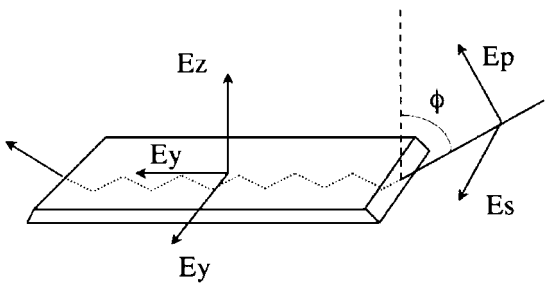

Fig. 6. Coordinate system for the polarized spectroscopy. ϕ is incident light angle. The electric field of the evanescent wave exists in 3 axes (x, y, z).

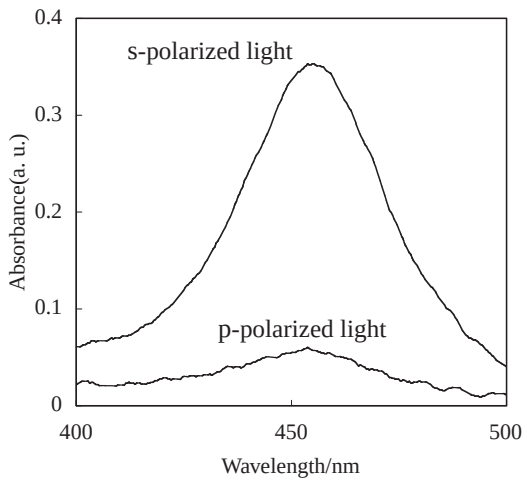

Fig. 7. Corrected polarized Vis-ATR spectrum of TMPyP adsorbed on the clay monolayer covered with water on waveguide quartz glass.

Estimation of Orientation Angle by Dichroic Measurement on a Waveguide. At first, in order to quantitatively estimate the orientation angle of the porphyrin molecules with respect to the nano-layered clay surface, the magnitude and the angle of the two transition moments (Soret band) of TMPyP, *cis*-DPyP, and *trans*-DPyP were calculated as follows. Geometry optimization was carried out with Gaussian03 (B3LYP/6-31G*).[51] Then, the excitation energy was calculated with MOS-F5.0A (CNDO/S). The calculation results for each porphyrin are shown in Fig. 9. It was found that the two transition moments of TMPyP, *cis*-DPyP, and *trans*-DPyP were almost orthogonal (89.9, 90.3, and 85.5°) and had equal magnitude.

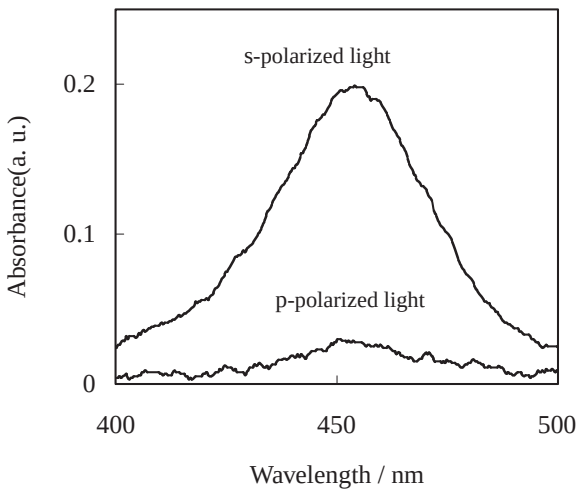

Fig. 8. Corrected polarized Vis-ATR spectrum of *cis*-DPyP adsorbed on the clay monolayer covered with water on waveguide quartz glass.

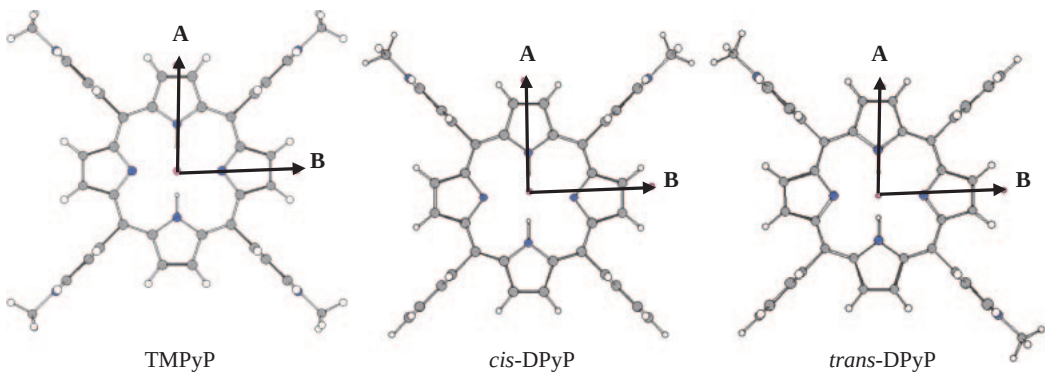

Fig. 9. Optimized geometry of each porphyrin molecule (calculated by Gaussian 03) and their transition moments (calculated by MOS-F5.0A). The transition moments A and B are nearly orthogonal.

The transition moments were directed along the N–H/N–H, and the N/N axes, respectively (Fig. 9). The relative strength and angle between the two transition moments were essentially not affected by the dihedral angle change between the porphyrin ring and the peripheral aromatic ring.

Derivation of Expression for Orientation Angle Analysis for the Porphyrin Molecule. In the case of the evanescent wave, the electric field exists along 3 axes (x, y, z) (Fig. 6). The x-axis is parallel to the direction of light propagation, the y-axis is perpendicular to the direction of light propogation, and the z-axis is parallel to the interface normal.

At the interface ($z = 0$), the electric field strength in each direction (E_{x0}, E_{y0}, E_{z0}) can be represented as Eqs. 1a–1c.[30–36]

$$E_{x0} = \frac{2\cos\varphi(\sin^2\varphi - n_{31}^2)^{1/2}}{\{(1-n_{31}^2)[(1+n_{31}^2)\sin^2\varphi - n_{31}^2]\}^{1/2}}, \tag{1a}$$

$$E_{y0} = \frac{2i\cos\varphi}{(1-n_{31}^2)^{1/2}}, \tag{1b}$$

$$E_{z0} = \frac{2in_{32}^2\cos\varphi\sin\varphi}{\{(1-n_{31}^2)[(1+n_{31}^2)\sin^2\varphi - n_{31}^2]\}^{1/2}}, \tag{1c}$$

where φ is the angle between internally reflected light and the surface normal, $n_{31} = n_3/n_1$, $n_{32} = n_3/n_2$, and n_1, n_2, and n_3 are the refractive indices of the waveguide (1.47), clay (1.52),[37] and solvent, respectively. In the present system, the density of porphyrin molecule on the waveguide was very low, and the molecular size was much smaller than the wavelength of monitor light. Thus, the effect of reflection and double reflection of porphyrin could be neglected like in usual ATR measurements.[38,52]

The dichroic ratio can be estimated with the use of polarized light.[30–36,38] A_p/A_s can be determined from Eq. 2, because the x- and z-components of the electric field and the y-component of the electric field correspond to p-polarized light and s-polarized light, respectively.

$$\frac{A_p}{A_s} = \frac{k_x {E_{x0}}^2 + k_z {E_{z0}}^2}{k_y {E_{y0}}^2}, \tag{2}$$

where k_x, k_y, k_z are the component values of the extinction coefficient. Because the porphyrin molecule has two orthogonal transition moments (Fig. 10), as previously mentioned, the equation of dichroic ratio can be modified to Eq. 3.

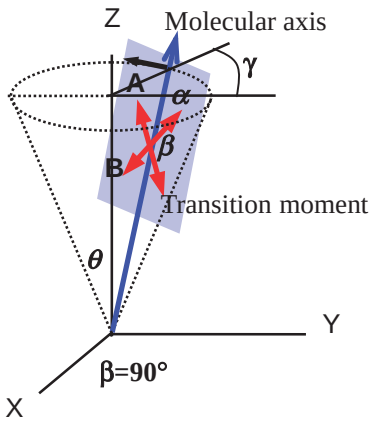

Fig. 10. Relationship between the coordinate system and the porphyrin molecule on the clay surfaces. θ is the angle between the z-axis and the molecular axis. α is the angle between the molecular axis and the transition moment A. β is the angle between the transition moments.

$$\frac{A_p}{A_s} = \frac{((k_{x\alpha 0} + k_{x\alpha 90} + k_{x\beta 0} + k_{x\beta 90}){E_{x0}}^2 + (k_{z\alpha 0} + k_{z\alpha 90} + k_{z\beta 0} + k_{z\beta 90}){E_{z0}}^2}{(k_{y\alpha 0} + k_{y\alpha 90} + k_{y\beta 0} + k_{y\beta 90}){E_{y0}}^2}, \tag{3}$$

where the subscript α indicates the angle between the transition moment A and the molecular axes, and β indicates the angle between the two transition moments B (Fig. 10). The subscripts 0 and 90 represent the perpendicular and parallel parts of the transition moment with respect to the molecular axis in the molecular plane. Each of the extinction coefficients $(k_{x0}, k_{y0}, k_{z0}, k_{x90}, k_{z90})$ can be represented as Eqs. 4a–4d, which were obtained by integration on the x–y plane (i.e., about the z-axis) in Fig. 10 in order to include all possible orientations with respect to the z-axis.

$$k_{x0} = k_{y0} = K\pi M^2\cos^2\alpha\sin^2\theta, \tag{4a}$$

$$k_{z0} = 2K\pi M^2\cos^2\alpha\cos^2\theta, \tag{4b}$$

$$k_{x90} = k_{y90} = K\pi M^2\sin^2\alpha, \tag{4c}$$

$$k_{z90} = 0. \tag{4d}$$

By applying Eqs. 4a–4d. to Eq. 3, Eq. 5, which represents the relationship between the orientation angle of the molecules to the normal (θ) and A_p/A_s was derived.

$$\theta = \arcsin\sqrt{\frac{\{\sin^2\alpha + \sin^2(\alpha+\beta)\}{E_x}^2 - \frac{A_p}{A_s}\{\sin^2\alpha + \sin^2(\alpha+\beta)\}{E_y}^2 + 2\{\cos^2\alpha + \cos^2(\alpha+\beta)\}{E_z}^2}{-\{\cos^2\alpha + \cos^2(\alpha+\beta)\}{E_x}^2 + \frac{A_p}{A_s}\{\cos^2\alpha + \cos^2(\alpha+\beta)\}{E_y}^2 + 2\{\cos^2\alpha + \cos^2(\alpha+\beta)\}{E_z}^2}}. \tag{5}$$

The α and β values were assumed to be 45 and 90° from the results of the calculation of the transition moment and from the positions of the cationic sites of the porphyrin molecule.

Figure 11 shows the relationship between the orientation angle of the molecules to the normal (θ) and A_p/A_s under the conditions simulated by Eq. 5.

Determination of Orientation Angle from the Results of Dichroic Measurements on the Waveguide. From the Vis-ATR spectra, the values of A_p/A_s for TMPyP/clay, *cis*-DPyP/clay, and *trans*-DPyP/clay were 0.16, 0.13, and 0.13, respectively. The orientation angle was determined by applying Fig. 11 to these values, and they did not exceed 5°. These

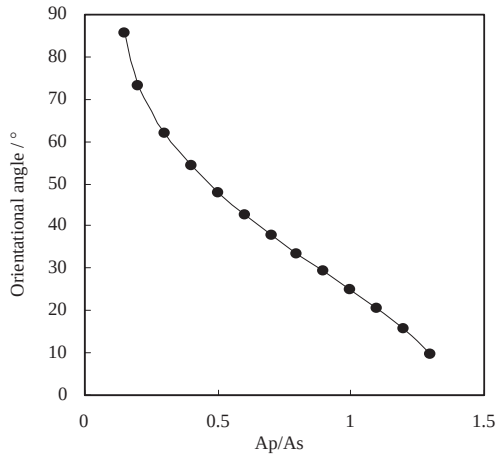

Fig. 11. Orientation angle (θ) versus observed A_p/A_s.

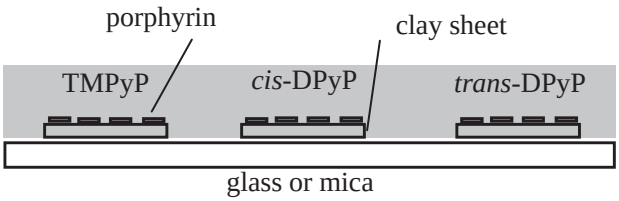

Fig. 12. Schematic view of the porphyrin–clay–glass/mica complex (side view).

results quantitatively indicate that the tetracationic and dicationic porphyrins adsorb on the nano-layered compound surface in an essentially parallel orientation with respect to the nano-layer clay surface in water.

Conclusion

AFM observations indicated that single clay sheets adsorbed on mica and glass substrates in a flat orientation. Vis-ATR spectra of clay–porphyrin complexes on a quartz waveguide were successfully observed, despite the presence of only a single monolayer of clay–porphyrin complex adsorbed on the substrate. PV-ATR spectroscopy indicated that both tetracationic and dicationic porphyrin molecule adsorbed parallel to the glass plate in water. From these observations, we conclude that the porphyrin molecules adsorb on the clay sheets in a flat orientation, as shown in Fig. 12.

The PV-ATR measurement proved to be a good technique for the analysis of the orientation of molecules on layered materials, specifically layered minerals. Since the sensitivity of the PV-ATR measurement is very high, due to the repeated total reflectance in the waveguide, it is possible to measure monolayer samples. In such samples, the glass substrate and the clay sheets should be completely parallel. The perfect coplanarity of the glass substrate and clay sheet is essential to obtain precise information on the molecular orientation on the clay surface. The PV-ATR measurements fulfill these conditions well. The clay mineral afforded a very flat surface as a chemical reaction platform or substrate to construct structure-regulated materials. Thus, the combination of clay minerals as platforms and PV-ATR as an analytical technique is a powerful tool for the development of nanotechnology and materials science.

This work has been partly supported by a Grant-in-Aid for Exploratory Research and Scientific Research on Priority Areas (417), Research Fellowships of the Japan Society for the Promotion of Science for Young Scientists, and a Grant-in-Aid for Young Scientists (B) from the Ministry of Education, Culture, Sports, Science and Technology (MEXT) of the Japanese Government.

References

1 J. K. Thomas, *Acc. Chem. Res.* **1988**, *21*, 275.
2 J. K. Thomas, *Chem. Rev.* **1993**, *93*, 301.
3 M. Ogawa, K. Kuroda, *Chem. Rev.* **1995**, *95*, 399.
4 K. Takagi, T. Shichi, in *Solid State and Surface Photochemistry*, ed. by V. Ramamurthy, K. S. Schanze, Marcel Dekker, New York, **2000**, Vol. 5, p. 31.
5 a) S. Takagi, M. Eguchi, D. A. Tryk, H. Inoue, *J. Photochem. Photobiol., C* **2006**, *7*, 104. b) S. Takagi, M. Eguchi, H. Inoue, *Langmuir* **2006**, *22*, 1406. c) S. Takagi, M. Eguchi, T. Yui, H. Inoue, *Clay Sci.* **2006**, *12*, 82.
6 Y. Umemura, Y. Einaga, A. Yamagishi, *Mater. Lett.* **2004**, *58*, 2472.
7 A. Czímerová, L. Jankovič, J. Bujdák, *J. Colloid Interface Sci.* **2004**, *274*, 126.
8 H. Lindgreen, J. Garnas, P. L. Hansen, F. Besenbacher, E. Lagsgaard, I. Stensgaard, S. A. C. Gould, P. K. Hansma, *Am. Mineral.* **1991**, *76*, 1218.
9 B. van Duffel, R. A. Schoonheydt, C. P. M. Grim, F. C. De Schryver, *Langmuir* **1999**, *15*, 7520.
10 R. D. Piner, T. T. Xu, F. T. Fisher, Y. Qiao, R. S. Ruoff, *Langmuir* **2003**, *19*, 7995.
11 Y. Umemura, A. Yamagishi, R. Schoonhydt, A. Persoons, F. De Schryver, *J. Am. Chem. Soc.* **2002**, *124*, 992.
12 R. H. A. Ras, C. T. Johnston, E. I. Franses, R. Ramaekers, G. Maes, P. Foubert, F. C. De Schryver, R. A. Schoonheydt, *Langmuir* **2003**, *19*, 4295.
13 *The Porphyrin Handbook*, ed. by K. M. Kadish, K. M. Smith, R. Guilard, Academic Press, New York, **1999**.
14 S. Takagi, H. Inoue, in *Multimetallic and Macromolecular Inorganic Photochemistry*, ed. by V. Ramamurthy, K. S. Schanze, Marcel Dekker, New York, **1999**, Vol. 6, p. 215.
15 V. G. Kuykendall, J. K. Thomas, *Langmuir* **1990**, *6*, 1350.
16 Z. Chernia, D. Gill, *Langmuir* **1999**, *15*, 1625.
17 S. Takagi, T. Shimada, M. Eguchi, T. Yui, H. Yoshida, D. A. Tryk, H. Inoue, *Langmuir* **2002**, *18*, 2265.
18 G. Villemure, C. Detellier, A. G. Szabo, *J. Am. Chem. Soc.* **1986**, *108*, 4658.
19 G. Villemure, C. Detellier, A. G. Szabo, *Langmuir* **1991**, *7*, 1215.
20 S. Takagi, T. Shimada, T. Yui, H. Inoue, *Chem. Lett.* **2001**, 128.
21 S. Takagi, D. A. Tryk, H. Inoue, *J. Phys. Chem. B* **2002**, *106*, 5455.
22 M. Eguchi, S. Takagi, H. Tachibana, H. Inoue, *J. Phys. Chem. Solid* **2004**, *65*, 403.
23 L. Ukrainczyk, M. Chibwe, T. J. Pinnavaia, S. A. Boyd, *Environ. Sci. Technol.* **1995**, *29*, 439.
24 G. Binnig, C. F. Quate, C. Gerber, *Phys. Rev. Lett.* **1986**, *56*, 930.
25 P. K. Hansma, V. B. Elings, O. Marti, C. E. Bracker, *Science* **1988**, *242*, 209.
26 H. Akutsu, Y. Kyogoku, H. Nakahara, K. Fukuda, *Chem.*

Phys. Lipids **1975**, *15*, 222.
27 R. Sasai, N. Shinya, T. Shichi, K. Takagi, K. Gekko, *Langmuir* **1999**, *15*, 413.
28 R. D. B. Fraser, *J. Chem. Phys.* **1953**, *21*, 1511.
29 D. S. Walker, H. W. Hellinga, S. S. Saavedra, W. M. Reichert, *J. Phys. Chem.* **1993**, *97*, 10217.
30 N. J. Harrick, *J. Phys. Chem.* **1960**, *64*, 1110.
31 N. J. Harrick, *J. Opt. Soc. Am.* **1965**, *55*, 851.
32 U. P. Fringeli, *Z. Naturforsch., C: Biosci.* **1977**, *32*, 20.
33 R. Ishiguro, N. Kimura, S. Takahashi, *Biochemistry* **1993**, *32*, 9792.
34 J. W. Brauner, R. Mendelsohn, F. G. Prendergast, *Biochemistry* **1987**, *26*, 8151.
35 Y. L. Cheng, D. N. Batchelder, S. D. Evans, J. R. Henderson, *J. Phys. Chem. B* **1998**, *102*, 5309.
36 T. E. Plowman, S. S. Saavedra, W. M. Reichert, *Biomaterials* **1998**, *19*, 341.
37 C. Klein, *The Manual of Mineral Science*, 22nd ed., John Wiley & Sons, Inc., New York, 2001, p. 641.
38 P. H. Axelsen, M. J. Citra, *Prog. Biophys. Mol. Biol.* **1996**, *66*, 227.
39 M. Era, K. Miyake, Y. Yoshida, K. Yase, *Thin Solid Films* **2001**, *393*, 24.
40 O. Ohtani, T. Furukawa, R. Sasai, E. Hayashi, T. Shichi, T. Yui, K. Takagi, *J. Mater. Chem.* **2004**, *142*, 196.
41 Z. Tong, T. Shichi, K. Oshika, K. Takagi, *Chem. Lett.* **2002**, 876.
42 R. Sasai, T. Fujita, N. Iyi, H. Itoh, K. Takagi, *Langmuir* **2002**, *18*, 6578.
43 O. Ohtani, R. Sasai, T. Adachi, I. Hatta, K. Takagi, *Langmuir* **2002**, *18*, 1165.
44 R. Sasai, H. Itoh, I. Shindachi, T. Shichi, K. Takagi, *Chem. Mater.* **2001**, *13*, 2012.
45 K. Sonobe, K. Kikuta, K. Takagi, *Chem. Mater.* **1999**, *11*, 1089.
46 Y. Kaneko, N. Iyi, J. Bujdak, R. Sasai, T. Fujita, *J. Mater. Res.* **2003**, *18*, 2639.
47 J. Bujdak, N. Iyi, Y. Kaneko, R. Sasai, *Clay Miner.* **2003**, *38*, 559.
48 R. Sasai, N. Iyi, T. Fujita, K. Takagi, H. Itoh, *Chem. Lett.* **2003**, *32*, 550.
49 A. L. Lucia, T. Yui, R. Sasai, S. Takagi, K. Takagi, H. Yoshida, D. G. Whitten, H. Inoue, *J. Phys. Chem. B* **2003**, *107*, 3789.
50 N. Iyi, R. Sasai, T. Fujita, T. Deguchi, T. Sota, F. Lopez Arbeloa, K. Kitamura, *Appl. Clay Sci.* **2002**, *22*, 125.
51 M. J. Frisch, G. W. Trucks, H. B. Schlegel, G. E. Scuseria, M. A. Robb, J. R. Cheeseman, J. A. Montgomery, Jr., T. Vreven, K. N. Kudin, J. C. Burant, J. M. Millam, S. S. Iyengar, J. Tomasi, V. Barone, B. Mennucci, M. Cossi, G. Scalmani, N. Rega, G. A. Petersson, H. Nakatsuji, M. Hada, M. Ehara, K. Toyota, R. Fukuda, J. Hasegawa, M. Ishida, T. Nakajima, Y. Honda, O. Kitao, H. Nakai, M. Klene, X. Li, J. E. Knox, H. P. Hratchian, J. B. Cross, V. Bakken, C. Adamo, J. Jaramillo, R. Gomperts, R. E. Stratmann, O. Yazyev, A. J. Austin, R. Cammi, C. Pomelli, J. W. Ochterski, P. Y. Ayala, K. Morokuma, G. A. Voth, P. Salvador, J. J. Dannenberg, V. G. Zakrzewski, S. Dapprich, A. D. Daniels, M. C. Strain, O. Farkas, D. K. Malick, A. D. Rabuck, K. Raghavachari, J. B. Foresman, J. V. Ortiz, Q. Cui, A. G. Baboul, S. Clifford, J. Cioslowski, B. B. Stefanov, G. Liu, A. Liashenko, P. Piskorz, I. Komaromi, R. L. Martin, D. J. Fox, T. Keith, M. A. Al-Laham, C. Y. Peng, A. Nanayakkara, M. Challacombe, P. M. W. Gill, B. Johnson, W. Chen, M. W. Wong, C. Gonzalez, J. A. Pople, *Gaussian 03*, Gaussian Inc., Wallingford CT, **2004**.
52 V. Koppaka, P. H. Axelsen, *Langmuir* **2001**, *17*, 6309.